

Modeling and Parameter Design of Thyristor-Controlled LC -Coupled Hybrid Active Power Filter (TCLC-HAPF) for Unbalanced Compensation

Lei Wang, Chi-Seng Lam, *Senior Member, IEEE*, and Man-Chung Wong, *Senior Member, IEEE*

Abstract—In this paper, a new modeling and parameter design method for the thyristor-controlled LC -coupled hybrid active power filter (TCLC-HAPF) is proposed, which includes the analysis of the inner flowed three-phase unbalanced power during unbalanced condition. Different from the conventional method which ignores the inner flowed three-phase unbalanced power, the proposed design method can achieve better performance during unbalanced compensation. To verify the validity and advantages of the proposed modeling and parameter design method of TCLC-HAPF, the mathematical analysis, representative simulation and experimental results for compensating different unbalanced loading situation are presented in comparison with the conventional design method.

Index Terms—Active power, current harmonics, reactive power, thyristor-controlled LC (TCLC) compensator, thyristor-controlled LC -coupling hybrid active power filter (TCLC-HAPF), unbalanced compensation.

I. INTRODUCTION

UNBALANCED problem is considered as one of the major power quality (PQ) problems, which is mainly caused by connecting of the unsymmetrical or single-phase loads to the power system. Researchers have well noticed the importance of addressing unbalanced problem by continuously improving the structures and control methods of different PQ compensators [1]–[18]. From the late 1970s onwards, the static Var compen-

Manuscript received April 15, 2016; revised July 30, 2016 and September 17, 2016; accepted October 11, 2016. Date of publication November 3, 2016; date of current version February 9, 2017. This work was supported in part by the Macau Science and Technology Development Fund (FDCT) under Grant FDCT 109/2013/A3 and in part by the Research Committee of the University of Macau under Grant MRG012/WMC/2015/FST, Grant MYRG2015-00009-FST, and Grant MYRG2015-00030-AMSV. (Corresponding author: Chi-Seng Lam.)

L. Wang is with the Department of Electrical and Computer Engineering, Faculty of Science and Technology, University of Macau, Macao 999078, China (e-mail: jordanwanglei@gmail.com).

C.-S. Lam is with the State Key Laboratory of Analog and Mixed Signal VLSI, University of Macau, Macao 999078, China (e-mail: cslam@umac.mo; C.S.Lam@ieee.org).

M.-C. Wong is with the Department of Electrical and Computer Engineering, Faculty of Science and Technology and the State Key Laboratory of Analog and Mixed Signal VLSI, University of Macau, Macao 999078, China (e-mail: mcwong@umac.mo).

Color versions of one or more of the figures in this paper are available online at <http://ieeexplore.ieee.org>.

Digital Object Identifier 10.1109/TIE.2016.2625239

sators (SVCs) have been used to balance the system in some key locations of power networks [1]. To control the SVCs for unbalanced compensation, different control strategies have been proposed in [1]–[4]. Individual phase control scheme and a poly-phase Newton–Raphson power flow program have been reported in [1] and [2], respectively, to control the power flow and balance the unbalanced power systems. In [3], the feedback control and feedforward control algorithms are developed and compared. To reduce the harmonic current contents in an unbalanced power system, the combination of fixed capacitor thyristor-controlled reactor (TCR) and series passive power filter, and thyristor-controlled LC (TCLC) filter have been introduced in [4] and [5]. From the year of 1976 onwards, active power filters (APFs) have gradually replaced the SVCs for unbalanced compensation [6]–[10]. Moreover, their control methods have been continuously improved by considering different operation voltage and current conditions. In recent two years, by applying APFs for unbalanced compensation, many different control methods have been reported to calculate the current or voltage references for compensation such as direct power control [6], [7], repetitive control [8], artificial neural networks-based control [9] $i_d - i_q$ control [10], etc. However, due to its structure limitations, the active inverter part of APF needs to keep at a large rating to perform unbalanced compensation, which drives up their cost. In 2003, LC -coupling hybrid active power filters (HAPFs) were proposed to reduce the size and cost of active inverter part compared with APFs [11]–[13]. However, the HAPF has a quite narrow compensation range, which limits its unbalanced compensation ability. To reduce the voltage or current rating of APF and keep good compensation ability simultaneously, different combinations of SVCs in series/parallel with APFs (SVC//APFs [14] and SVC+APFs [15]–[19]) have been proposed from 2008 onwards. Among them, the thyristor-controlled LC -coupled hybrid active power filter (TCLC-HAPF) [17]–[19] as one of the SVC+APF structures has distinct characteristics of wide compensation range and low active inverter capacity. Therefore, the TCLC-HAPF has high potential to be further developed for unbalanced compensation.

For the above discussed PQ compensators, their modeling and parameter design methods are different because the passive components play different roles in their different structures. The coupling inductor of the APF is designed to filter out the current

TABLE I
DIFFERENT PQ COMPENSATORS AND THEIR CORRESPONDING MODELING AND PARAMETER DESIGN METHODS

| | Year | Unbalanced modeling | Parameter design method |
|---|---------------|---------------------------------|--|
| SVCs [1]–[4] | 1960s | Lack of study | Maximum phase of premeasured Q_{Lx} |
| APFs [6]–[10] | 1976 | Single-phase modeling | Inverter output current ripples (coupling L design) Q_{Lx} and harmonic compensation (V_{DC} design) |
| HAPFs [11]–[13] | 2003 | Single-phase modeling | Average of premeasured Q_{Lx} and dominated harmonic current order (coupling LC design) Residual Q_{Lx} and harmonic compensation (V_{DC} design) |
| SVC//APF [14] SVC+APF [15]–[16] | 2000s | Single-phase modeling | Maximum phase of premeasured Q_{Lx} (SVC design) Inverter output current ripples (APF coupling L design) Residual Q_{Lx} and harmonic compensation (APF V_{DC} design) |
| Conventional TCLC-HAPF design [17]–[19] | 2014 and 2106 | Single-phase modeling | Maximum phase of premeasured Q_{Lx} (SVC design) Residual Q_{Lx} and harmonic compensation (V_{DC} design) |
| Proposed TCLC-HAPF design | 2016 | Unbalanced three-phase modeling | Inner-flow unbalanced power and maximum phase of premeasured Q_{Lx} (SVC design) Harmonic compensation only (V_{DC} design) |

ripples generated by power switches [6]–[10]. And its active inverter part is used to compensate the load reactive power, current harmonics, and unbalanced power. In comparison, the coupling inductor and capacitor (LC) of the HAPF are normally designed to compensate the average fundamental reactive power and the dominated harmonic current order of the loading [11]–[13], so that its active inverter part rating can be significantly reduced. The different structures of SVCs and SVC part of the combined systems [SVC//APFs and SVC+APFs (TCLC-HAPF)] are proposed for dynamic reactive power compensation [1]–[4], [14]–[18]. Thus, the parameter design methods are usually designed to cover the premeasured maximum reactive power only, while the inner flowed three-phase unbalanced power has not been taken into consideration. For unbalanced loading compensation, the above conventional parameter design methods [1]–[4], [14]–[18] may lead the PQ compensators fall outside their compensation range, thus deteriorates their compensation performance.

In this paper, a three-phase modeling and parameter design method for TCLC-HAPF is proposed in order to overcome the aforementioned compensation problem during unbalanced loading situation. Table I summarizes the different PQ compensators and their modeling and parameter design methods.

In the following, the circuit configuration of the three-phase three-wire TCLC-HAPF is presented. Then, the three-phase modeling for unbalanced compensation analysis is proposed in Section II. Based on the circuit configuration and modeling, the parameter design method is proposed and discussed under different types of unbalanced loading in Section III. To verify the

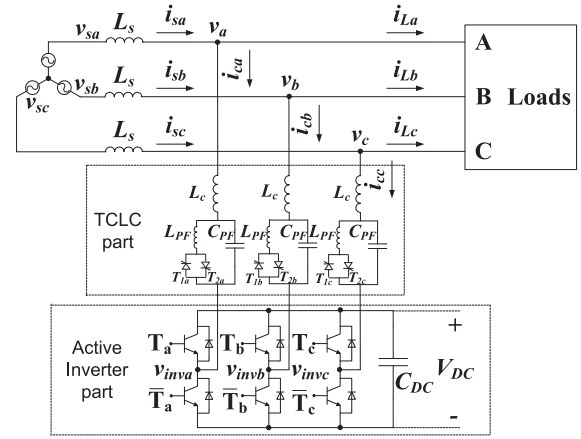


Fig. 1. Circuit configurations of the TCLC-HAPF.

proposed parameter design method, the simulation case studies are presented in Section IV in comparison to the conventional design method [18]. In Section V, representative experimental results are given. Finally, conclusion is drawn in Section VI.

II. CIRCUIT CONFIGURATION AND MODELING OF THE THREE-PHASE TCLC-HAPF

The system topology of a three-phase three-wire TCLC-HAPF is provided in Fig. 1. The TCLC part of the TCLC-HAPF consists of a coupling inductor L_c , a parallel capacitive C_{PF} , and a TCR with an inductor L_{PF} . The active inverter part is a two-level voltage-source inverter with a dc-link capacitor C_{DC} . v_{sx} , v_x , and v_{invx} are the source voltage, load voltage, and inverter output voltage, respectively, where the subscript “ x ” denotes phase $x = a, b, c$; i_{sx} , i_{Lx} , and i_{cx} are source current, load current, and compensating current, respectively.

The active inverter part can be considered as the adjustable active impedance to improve the TCLC part fundamental and harmonic current compensation ability [20], [21]. Therefore, the three-phase modeling for TCLC-HAPF unbalanced compensation analysis is proposed in Fig. 2. At the fundamental frequency [see Fig. 2(a)], the active impedance X_{ACTxf} is used to help the TCLC part impedance X_{af} to compensate fundamental reactive power and balance active power. At the harmonic frequency [see Fig. 2(b)], the active impedance X_{ACTxh} changes the equivalent TCLC-HAPF impedance to be zero, so that the load harmonic current will not pollute the source side. The fundamental and harmonic active impedance X_{ACTxf} and X_{ACTxh} are proportional to the inverter voltage. To keep active inverter working at low rating, X_{ACTxf} and X_{ACTxh} need to be designed as small as possible.

III. PROPOSED TCLC-HAPF PARAMETER DESIGN FOR UNBALANCED COMPENSATION

In this section, a parameter design method is discussed and explained into four parts. In Section III-A, the relationship between the required TCLC-HAPF fundamental impedances ($X_{af} + X_{ACTxf}$) and the load powers is deduced based on power flow analysis. The parameter design of the re-

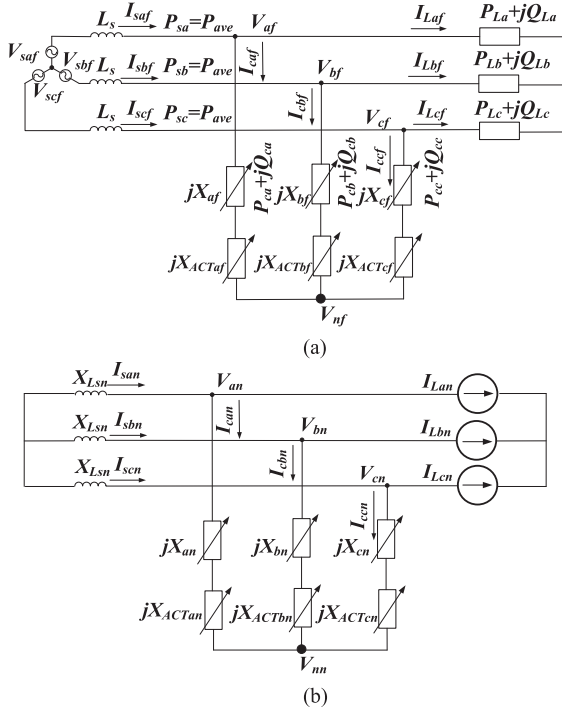


Fig. 2. Three-phase TCLC-HAPF modeling for unbalanced compensation: (a) at fundamental frequency and (b) at harmonic frequency.

quired fundamental dc-link voltage V_{DCf} , C_{PF} , and L_{PF} is proposed under the fundamental frequency consideration for three different kinds of unbalanced loading. In Section III-B, the parameter design of the required harmonic dc-link voltage V_{DCh} is proposed under harmonic frequency consideration. In Section III-C, the design of L_c is given. In Section III-D, a summary table of TCLC-HAPF parameter design is drawn in Table II.

A. Design of V_{dcf} , C_{PF} , and L_{PF} Based on Power Flow Analysis Under Fundamental Frequency Consideration

Referring to Fig. 2(a), the required TCLC-HAPF impedance ($X_{xf} + X_{ACTxf}$) can be calculated by applying Ohm's law as follows:

$$jX_{xf} + jX_{ACTxf} = (\vec{V}_{xf} - \vec{V}_{nf}) / \vec{I}_{cxf} \quad (1)$$

where \vec{V}_{xf} and \vec{I}_{cxf} are the fundamental load voltage and compensating current phasors, respectively, where x stands for phase a , b , and c . \vec{V}_{nf} is the fundamental common point voltage. By using Kirchhoff's circuit laws, the compensating current relationship can be expressed as follows:

$$\vec{I}_{caf} + \vec{I}_{cbf} + \vec{I}_{ccf} = \frac{\vec{V}_a - \vec{V}_{nf}}{jX_{af} + jX_{ACTaf}} + \frac{\vec{V}_b - \vec{V}_{nf}}{jX_{bf} + jX_{ACTbf}} + \frac{\vec{V}_c - \vec{V}_{nf}}{jX_{cf} + jX_{ACTcf}} = 0. \quad (2)$$

TABLE II
PROPOSED PARAMETER DESIGN OF TCLC-HAPF UNDER THREE DIFFERENT TYPES OF LOADING

| Parameter | Load types | C_{PF} design | L_{PF} design |
|--|------------------------------------|--|--|
| Design L_{PF} and C_{PF} | Unbalanced inductive loads | $\frac{1}{\omega^2 L_c - \omega X_{xf}} \leq C_{PF} < \frac{1}{\omega^2 L_c}$ (18) | $L_{PF} < \frac{1}{\omega^2 C_{PF}}$ (16) |
| | Unbalanced capacitive loads | $C_{PF} < \frac{1}{\omega^2 L_c}$ (15) | $L_{PF} \leq \frac{X_{xf} - \omega L_c}{\omega^2 X_{xf} C_{PF} - \omega^3 L_c C_{PF} + \omega}$ (22) |
| | Mixed inductive & capacitive loads | $\frac{1}{\omega^2 L_c - \omega X_{xf}} \leq C_{PF} < \frac{1}{\omega^2 L_c}$ (18) | $L_{PF} \leq \frac{X_{xf} - \omega L_c}{\omega^2 X_{xf} C_{PF} - \omega^3 L_c C_{PF} + \omega}$ (22) |
| The final C_{PF} and L_{PF} can be expressed as: | | | |
| | | $C_{PF} = \max(C_{PF} _{X_{af}}, C_{PF} _{X_{bf}}, C_{PF} _{X_{cf}})$ (19) | |
| | | $L_{PF} = \min(L_{PF} _{X_{af}}, L_{PF} _{X_{bf}}, L_{PF} _{X_{cf}})$ (23) | |
| Design L_c | | $L_c \geq \frac{V_{DC}}{8 \cdot f_s \cdot \Delta i_{L_{max}}}$ (29) | |
| Design V_{DC} | | $V_{DC} = \sqrt{V_{DCf}^2 + V_{DCh}^2} = \max\left(\sqrt{6} \sqrt{\sum_{n=2}^{\infty} (X_{an} \cdot I_{Lan})^2}, \sqrt{6} \sqrt{\sum_{n=2}^{\infty} (X_{bn} \cdot I_{Lbn})^2}, \sqrt{6} \sqrt{\sum_{n=2}^{\infty} (X_{cn} \cdot I_{Lcn})^2}\right)$ (28) | |

X_{xf} is obtained from (1) and x stands for phase a , b and c .

$$\begin{bmatrix} X_{af} \\ X_{bf} \\ X_{cf} \end{bmatrix} = \begin{bmatrix} \frac{3\vec{V}_x^2 (Q_{Lc} - Q_{Lb} - Q_{La})^{-1} (Q_{Lb} - Q_{La} - Q_{Lc})^{-1}}{(Q_{Lc} - Q_{Lb} - Q_{La})^{-1} + (Q_{La} - Q_{Lb} - Q_{Lc})^{-1} + (Q_{Lb} - Q_{La} - Q_{Lc})^{-1}} \\ \frac{3\vec{V}_x^2 (Q_{Lc} - Q_{Lb} - Q_{La})^{-1} (Q_{La} - Q_{Lb} - Q_{Lc})^{-1}}{(Q_{Lc} - Q_{Lb} - Q_{La})^{-1} + (Q_{La} - Q_{Lb} - Q_{Lc})^{-1} + (Q_{Lb} - Q_{La} - Q_{Lc})^{-1}} \\ \frac{3\vec{V}_x^2 (Q_{La} - Q_{Lb} - Q_{Lc})^{-1} (Q_{Lb} - Q_{La} - Q_{Lc})^{-1}}{(Q_{Lc} - Q_{Lb} - Q_{La})^{-1} + (Q_{La} - Q_{Lb} - Q_{Lc})^{-1} + (Q_{Lb} - Q_{La} - Q_{Lc})^{-1}} \end{bmatrix} \quad (11)$$

Simplifying (2), the expression of \vec{V}_{nf} can be obtained as follows:

$$\vec{V}_{nf} = \frac{(X_{bf} + X_{ACTbf})(X_{cf} + X_{ACTcf})}{X_{Eqf}} \cdot \vec{V}_{af} + \frac{(X_{cf} + X_{ACTcf})(X_{af} + X_{ACTaf})}{X_{Eqf}} \cdot \vec{V}_{bf} + \frac{(X_{af} + X_{ACTaf})(X_{bf} + X_{ACTbf})}{X_{Eqf}} \cdot \vec{V}_{cf} \quad (3)$$

where

$$X_{Eqf} = (X_{af} + X_{ACTaf})(X_{bf} + X_{ACTbf}) + (X_{bf} + X_{ACTbf})(X_{cf} + X_{ACTcf}) + (X_{cf} + X_{ACTcf})(X_{af} + X_{ACTaf}). \quad (4)$$

\vec{I}_{cxf} can be expressed in terms of \vec{V}_{xf} ($\vec{V}_x = \vec{V}_{xf}$ for v_x is assumed to be pure sinusoidal without harmonic components [11]–[13], [18]) and the compensating active and reactive power P_{cx} and Q_{cx} as follows:

$$\vec{I}_{cxf} = \left[(P_{cx} + jQ_{cx}) / \vec{V}_x \right]^* \quad (5)$$

where the note “*” denotes the conjugate. For unbalanced compensation, the TCLC-HAPF can provide the same amount of Q_{cx} as the loading required but with opposite directions and

balance the three-phase source active power to their average values $(P_{La} + P_{Lb} + P_{Lc})/3$ simultaneously. Thus, the compensating P_{cx} and Q_{cx} can be expressed as follows:

$$Q_{cx} = -Q_{Lx} \text{ and } P_{cx} = - \left(P_{Lx} - \frac{P_{La} + P_{Lb} + P_{Lc}}{3} \right). \quad (6)$$

Based on (1)–(6), the required TCLC-HAPF impedance ($X_{xf} + X_{ACTxf}$) can be deduced as (7), shown at the bottom of the page, where \bar{V}_x is the root-mean-square (rms) value of load voltage. From (7), the TCLC-HAPF impedances ($X_{xf} + X_{ACTxf}$) can be calculated based on Q_{Lx} and \bar{V}_x . With the premeasured variation ranges of Q_{Lx} , the required $X_{xf} + X_{ACTxf}$ can be obtained.

Referring to Fig. 2(a), the fundamental inverter voltage V_{invxf} can be obtained as follows:

$$V_{invxf} = X_{ACTxf} \cdot I_{cxf} \quad (8)$$

where X_{ACTxf} and I_{cxf} are the fundamental active impedance and compensating current, and I_{cxf} is design to compensate load fundamental reactive current i_{Lxfq} ($I_{cxf} = -I_{Lxfq}$). The relationship between the V_{invxf} and V_{DCxf} can be expressed as follows:

$$V_{DCxf} = \sqrt{6} \cdot V_{invxf}. \quad (9)$$

In (9), the scale of $\sqrt{6} (= \sqrt{3} \cdot \sqrt{2})$ can be explained by the following two reasons: 1) to transfer the phase voltage V_{invxf} to line-to-line voltage, the scale of $\sqrt{3}$ is required; and 2) to guarantee the sufficient V_{DCxf} , the peak value of fundamental inverter voltage needs to be considered $V_{invxf(p)} = \sqrt{2} \cdot V_{invxf}$.

Moreover, the final required V_{DCf} is designed to be the maximum value among each phase. Therefore, the final required V_{DCf} can be expressed as follows:

$$V_{DCf} = \max(\sqrt{6} \cdot V_{invaf}, \sqrt{6} \cdot V_{invbf}, \sqrt{6} \cdot V_{invcf}). \quad (10)$$

Based on (8)–(10), the X_{ACTxf} is directly proportional to the required V_{DCf} . The low dc-link voltage is one of the major advantages of TCLC-HAPF. This can be achieved when the value of X_{ACTxf} is designed to be zero ($X_{ACTxf} \approx 0$). In other words, the value of V_{DCf} is minimized ($V_{DCf} \approx 0$). With such minimum V_{DCf} design, the TCLC part is mainly used to compensate reactive power and balance the active power, while the active inverter part is mainly used to improve the harmonic compensation ability of TCLC part (discussed in the next part). Therefore, (7) can be simplified as (11), shown at the bottom of the page.

The TCLC part is an L_c (X_{Lc}) in series with a paralleled combination of a L_{PF} ($X_{L_{PF}}$) and a C_{PF} ($X_{C_{PF}}$), in which the X_{xf} can be deduced as (12), shown at the bottom of the page.

In (12), X_{Lc} , $X_{C_{PF}}$, and $X_{L_{PF}}$ are the fundamental impedances of L_c , C_{PF} , and L_{PF} . α_x is the firing angle of the thyristor. The TCLC part has two back-to-back connected thyristors T_{1x} and T_{2x} , and they are triggered alternately in every half-cycle. When $\alpha_x = 180^\circ$ (thyristors are opened for the whole cycle), the TCLC part has the maximum capacitive impedance $X_{Cap(Max)} (< 0)$. On the other hand, when the firing angle $\alpha_x = 90^\circ$ (one of thyristors is closed for whole cycle), the TCLC part has the minimum inductive impedance $X_{Ind(Min)} (> 0)$. Therefore, $X_{Cap(Max)}$ and $X_{Ind(Min)}$ can be

$$\begin{bmatrix} X_{af} + X_{ACTaf} \\ X_{bf} + X_{ACTbf} \\ X_{cf} + X_{ACTcf} \end{bmatrix} = \begin{bmatrix} \frac{3\bar{V}_x^2(Q_{Lc} - Q_{Lb} - Q_{La})^{-1}(Q_{Lb} - Q_{La} - Q_{Lc})^{-1}}{(Q_{Lc} - Q_{Lb} - Q_{La})^{-1} + (Q_{La} - Q_{Lb} - Q_{Lc})^{-1} + (Q_{Lb} - Q_{La} - Q_{Lc})^{-1}} \\ \frac{3\bar{V}_x^2(Q_{Lc} - Q_{Lb} - Q_{La})^{-1}(Q_{La} - Q_{Lb} - Q_{Lc})^{-1}}{(Q_{Lc} - Q_{Lb} - Q_{La})^{-1} + (Q_{La} - Q_{Lb} - Q_{Lc})^{-1} + (Q_{Lb} - Q_{La} - Q_{Lc})^{-1}} \\ \frac{3\bar{V}_x^2(Q_{La} - Q_{Lb} - Q_{Lc})^{-1}(Q_{Lb} - Q_{La} - Q_{Lc})^{-1}}{(Q_{Lc} - Q_{Lb} - Q_{La})^{-1} + (Q_{La} - Q_{Lb} - Q_{Lc})^{-1} + (Q_{Lb} - Q_{La} - Q_{Lc})^{-1}} \end{bmatrix} \quad (7)$$

$$\begin{bmatrix} X_{af} \\ X_{bf} \\ X_{cf} \end{bmatrix} = \begin{bmatrix} \frac{3\bar{V}_x^2(Q_{Lc} - Q_{Lb} - Q_{La})^{-1}(Q_{Lb} - Q_{La} - Q_{Lc})^{-1}}{(Q_{Lc} - Q_{Lb} - Q_{La})^{-1} + (Q_{La} - Q_{Lb} - Q_{Lc})^{-1} + (Q_{Lb} - Q_{La} - Q_{Lc})^{-1}} \\ \frac{3\bar{V}_x^2(Q_{Lc} - Q_{Lb} - Q_{La})^{-1}(Q_{La} - Q_{Lb} - Q_{Lc})^{-1}}{(Q_{Lc} - Q_{Lb} - Q_{La})^{-1} + (Q_{La} - Q_{Lb} - Q_{Lc})^{-1} + (Q_{Lb} - Q_{La} - Q_{Lc})^{-1}} \\ \frac{3\bar{V}_x^2(Q_{La} - Q_{Lb} - Q_{Lc})^{-1}(Q_{Lb} - Q_{La} - Q_{Lc})^{-1}}{(Q_{Lc} - Q_{Lb} - Q_{La})^{-1} + (Q_{La} - Q_{Lb} - Q_{Lc})^{-1} + (Q_{Lb} - Q_{La} - Q_{Lc})^{-1}} \end{bmatrix}. \quad (11)$$

$$\begin{bmatrix} X_{af}(\alpha_a) \\ X_{bf}(\alpha_b) \\ X_{cf}(\alpha_c) \end{bmatrix} = \begin{bmatrix} \frac{\pi X_{L_{PF}} X_{C_{PF}}}{X_{C_{PF}}(2\pi - 2\alpha_a + \sin 2\alpha_a) - \pi X_{L_{PF}}} + X_{Lc} \\ \frac{\pi X_{L_{PF}} X_{C_{PF}}}{X_{C_{PF}}(2\pi - 2\alpha_b + \sin 2\alpha_b) - \pi X_{L_{PF}}} + X_{Lc} \\ \frac{\pi X_{L_{PF}} X_{C_{PF}}}{X_{C_{PF}}(2\pi - 2\alpha_c + \sin 2\alpha_c) - \pi X_{L_{PF}}} + X_{Lc} \end{bmatrix} \quad (12)$$

expressed as follows:

$$X_{C_{ap}(\text{Max})} = X_{L_c} - X_{C_{PF}} = \omega L_c - 1/\omega C_{PF} \quad (13)$$

$$X_{\text{Ind}(\text{Min})} = \frac{X_{L_{PF}} X_{C_{PF}}}{X_{C_{PF}} - X_{L_{PF}}} + X_{L_c} = \frac{\omega L_{PF}}{1 - \omega^2 L_{PF} C_{PF}} + \omega L_c \quad (14)$$

where $\omega (= 2\pi f)$ is the angular frequency. To guarantee the TCLC part has inductive compensation range and capacitive compensation range, the basic conditions of $X_{C_{ap}(\text{Max})} < 0$ and $X_{\text{Ind}(\text{Min})} > 0$ need to be satisfied. Thus, from (13) and (14) the following relationships can be obtained:

$$C_{PF} < \frac{1}{\omega^2 L_c} \quad (15)$$

$$L_{PF} < \frac{1}{\omega^2 C_{PF}}. \quad (16)$$

In the following, the design of C_{PF} and L_{PF} will be separated into three different kinds of loading for discussion: 1) unbalanced inductive loads; 2) unbalanced capacitive loads; and 3) mixed inductive and capacitive loads.

- 1) For the unbalanced inductive loading compensation, the required TCLC impedance X_{xf} obtained in (11) is capacitive ($X_{xf} < 0$). To compensate inductive loads, the design maximum capacitive impedances $X_{C_{ap}(\text{Max})}$ in (13) are required to be equal to or larger than the required X_{xf} in (11). Therefore, the X_{xf} design criteria can be given as follows:

$$X_{xf} \leq X_{C_{ap}(\text{Max})} < 0. \quad (17)$$

Substituting (13) into (17), the design criteria of C_{PF} can be obtained as follows:

$$\frac{1}{\omega^2 L_c - \omega X_{xf}} \leq C_{PF} < \frac{1}{\omega^2 L_c} \quad (18)$$

where the final C_{PF} can be obtained as follows:

$$C_{PF} = \max(C_{PF}|_{X_{af}}, C_{PF}|_{X_{bf}}, C_{PF}|_{X_{cf}}). \quad (19)$$

To ensure the TCLC part can cover the entire inductive loading range, the compensating range needs to cover the capacitive boundary (left hand side term of (18)). Then, the TCLC inductance L_{PF} can be designed by (16) accordingly.

- 2) For unbalanced capacitive loads compensation, the required TCLC impedances X_{xf} in (11) are inductive ($X_{xf} > 0$). To compensate capacitive loads, the design minimum inductive impedances $X_{\text{Ind}(\text{min})}$ in (14) are required to be equal or smaller than X_{xf} . Therefore, the X_{xf} design criterion for each phase can be given as follows:

$$X_{xf} \geq X_{\text{Ind}(\text{Min})} > 0. \quad (20)$$

Substituting (14) into (20), the design criteria of L_{PF} can be obtained as follows:

$$\frac{L_c}{\omega^2 L_c C_{PF} - 1} < L_{PF} \leq \frac{X_{xf} - \omega L_c}{\omega^2 X_{xf} C_{PF} - \omega^3 L_c C_{PF} + \omega}. \quad (21)$$

Similarly, to ensure X_{xf} can cover the entire capacitive loading range, the compensating range needs to reach the inductive boundary. Then, C_{PF} can be designed by (15) accordingly.

However, with satisfying (15), the left-side boundary of (21) is a negative value, so that (21) can be further simplified as follows:

$$L_{PF} \leq \frac{X_{xf} - \omega L_c}{\omega^2 X_{xf} C_{PF} - \omega^3 L_c C_{PF} + \omega} \quad (22)$$

where the final L_{PF} can be obtained as follows:

$$L_{PF} = \min(L_{PF}|_{X_{af}}, L_{PF}|_{X_{bf}}, L_{PF}|_{X_{cf}}). \quad (23)$$

- 3) When the unbalanced loading is mixed (mixed inductive and capacitive loads), the phase load reactive power can be positive ($Q_{Lx} > 0$) or negative ($Q_{Lx} < 0$). Therefore, both (18) and (22) are required to be satisfied. If the $X_{xf} < 0$, the design criterion of C_{PF} can be obtained by substituting the calculated X_{xf} into (18). On the other hand, the design criterion of L_{PF} can be obtained by substituting the calculated $X_{xf} > 0$ into (22).

Based on previous analysis, the design of C_{PF} and L_{PF} under the different types of loads can be summarized in [Table II](#).

B. Design of V_{DCh} Based on Harmonic Frequency Analysis

Referred to the harmonic models in [Fig. 2\(b\)](#), the harmonic current circulating in the source is provided as follows:

$$I_{sxn} = \frac{X_{xn} + X_{ACTxn}}{X_{Lsn} + X_{xn} + X_{ACTxn}} \cdot I_{Lxn} \quad (24)$$

where I_{sxn} and I_{Lxn} are the source and load harmonic currents, respectively. X_{Lsn} is the harmonic source-side inductance. The purpose of the X_{ACTxn} is to reduce the harmonic currents flowing into the source side. Ideally, I_{sxn} can be reduced to be zero ($I_{sxn} = 0$). Therefore, X_{ACTxn} can be controlled to be

$$X_{ACTxn} = -X_{xn}. \quad (25)$$

In (25), X_{ACTxn} and X_{xn} are the harmonic active impedance and harmonic impedance of TCLC part. The absolute value of X_{ACTxn} and X_{xn} in each harmonic order can be expressed as follows:

$$\begin{aligned} |X_{ACTxn}(\alpha)| &= |X_{xn}(\alpha)| \\ &= \left| \frac{\pi(n\omega L_{PF})}{(2\pi - 2\alpha + \sin 2\alpha) - \pi(n\omega)^2 \cdot L_{PF} C_{PF}} + n\omega L_c \right| \end{aligned} \quad (26)$$

where n is the harmonic order. Based on (26), the absolute value of the $X_{xn}(n)$ and active impedance $X_{ACTxn}(n)$ under different harmonic order can be plotted as [Fig. 3](#).

The similar deduction steps to obtain V_{DCh} in (8)–(10) can also be used to deduce the required dc-link voltage V_{DCh} for

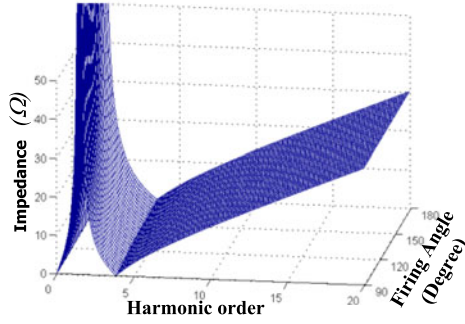


Fig. 3. Absolute value of X_{xn} and active impedance X_{ACTxn} under different harmonic orders.

harmonic current compensation as follows:

$$\begin{aligned}
 V_{DCh} &= \max \left(\sqrt{6} \cdot V_{invah}, \sqrt{6} \cdot V_{invbh}, \sqrt{6} \cdot V_{invch} \right) \\
 &= \max \left(\sqrt{6} \sqrt{\sum_{n=2}^{\infty} (X_{an} \cdot I_{Lan})^2}, \right. \\
 &\quad \left. \sqrt{6} \sqrt{\sum_{n=2}^{\infty} (X_{bn} \cdot I_{Lbn})^2}, \sqrt{6} \sqrt{\sum_{n=2}^{\infty} (X_{cn} \cdot I_{Lcn})^2} \right). \quad (27)
 \end{aligned}$$

In (27), I_{Lxn} is the load harmonic current, and the final V_{DC} in (28) is calculated as the sum of the square value of V_{DCf} in (10) and the square value of V_{DCh} in (27):

$$\begin{aligned}
 V_{DC} &= \sqrt{V_{DCf}^2 + V_{DCh}^2} = \max \left(\sqrt{6} \sqrt{\sum_{n=2}^{\infty} (X_{an} \cdot I_{Lan})^2}, \right. \\
 &\quad \left. \sqrt{6} \sqrt{\sum_{n=2}^{\infty} (X_{bn} \cdot I_{Lbn})^2}, \sqrt{6} \sqrt{\sum_{n=2}^{\infty} (X_{cn} \cdot I_{Lcn})^2} \right). \quad (28)
 \end{aligned}$$

In (28), I_{Lxn} is premeasured from the loading and X_{xn} is obtained from Fig. 3. To guarantee a sufficient V_{DC} for TCLC-HAPF compensation, V_{DC} is designed based on worst case I_{Lxn} during the premeasured period.

C. Design of L_c for Current Ripple Filtering

The purposed of L_c is to filter out the current ripple caused by the power switches of the active inverter part. The value of the L_c can be designed as follows:

$$L_c \geq \frac{V_{DC}}{8 \cdot f_s \cdot \Delta i_{Lc \max}} \quad (29)$$

where V_{DC} is the dc-link voltage, f_s is the switching frequency, and $\Delta i_{Lc \max}$ is the maximum allowed output current ripple value.

D. Summary of TCLC-HAPF Parameter Design

Based on previous discussions, the proposed parameter design method of TCLC-HAPF under three different types of

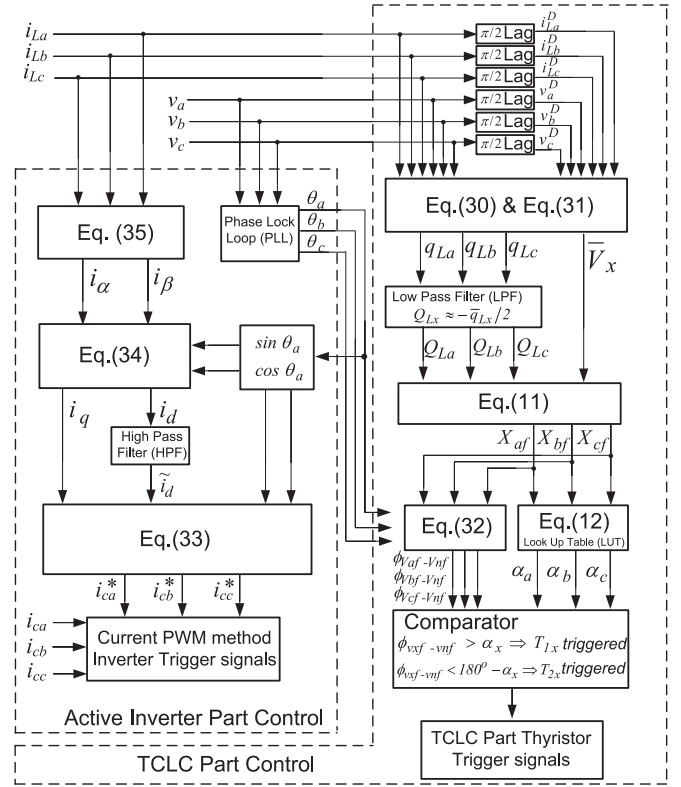


Fig. 4. Control block diagram of TCLC-HAPF.

loadings can be summarized in Table II. Once the ranges of I_{Lxn} and Q_{Lx} are premeasured, the TCLC-HAPF parameters can be designed accordingly by those equations in Table II.

IV. CONTROL STRATEGY OF TCLC-HAPF

In this section, the control strategy of TCLC-HAPF is separately into two parts: 1) the TCLC part; and 2) the active inverter part. The overall control block diagram of TCLC-HAPF is provided in Fig. 4.

A. TCLC Part Control

According to (11), the required TCLC impedance can be calculated through Q_{Lx} and $\bar{V}_x \cdot Q_{Lx}$ and \bar{V}_x can be calculated in real time as follows:

$$\begin{bmatrix} q_{La} \\ q_{Lb} \\ q_{Lc} \end{bmatrix} = \begin{bmatrix} v_a \cdot i_{La}^D - v_a^D \cdot i_{La} \\ v_b \cdot i_{Lb}^D - v_b^D \cdot i_{Lb} \\ v_c \cdot i_{Lc}^D - v_c^D \cdot i_{Lc} \end{bmatrix} \quad (30)$$

$$\bar{V}_x = \|v\| / \sqrt{3} = \sqrt{v_a^2 + v_b^2 + v_c^2} / \sqrt{3} \quad (31)$$

where v_x^D and i_{Lx}^D can be obtained by delaying v_x and i_{Lx} by a phase angle of 90° . q_{Lx} is the phase instantaneous reactive power. Then, $Q_{Lx} \approx -\bar{q}_{Lx}/2$ can be obtained by passing q_{Lx} in (30) through low-pass filters [13]. $\|v\|$ is the norm of three-phase instantaneous load voltage.

After obtaining $Q_{Lx} \approx -\bar{q}_{Lx}/2$, the required X_{xf} can be obtained from (11), that is controlled by the firing angle α_x through

(12). However, (12) does not have a closed-form solution. A lookup table has been installed to directly obtain the firing angle α_x with the known X_{xf} . By comparing the firing angle α_x with the phase angle of the voltage between TCLC part ($V_x - V_{nf}$), the trigger signals to control the thyristors can be obtained. The phase angle of voltage between TCLC part ($V_x - V_{nf}$) can be expressed as follows:

$$\begin{aligned} & \begin{bmatrix} \phi V_{af} - V_{nf} \\ \phi V_{bf} - V_{nf} \\ \phi V_{cf} - V_{nf} \end{bmatrix} \\ &= \begin{bmatrix} \theta_a - \tan^{-1} \left(\frac{X_{cf} - X_{bf}}{\sqrt{3}(X_{bf} + X_{cf})} \right) \\ \theta_b - \tan^{-1} \left(\frac{X_{af} - X_{cf}}{\sqrt{3}(X_{af} + X_{cf})} \right) \\ \theta_c - \tan^{-1} \left(\frac{X_{bf} - X_{af}}{\sqrt{3}(X_{bf} + X_{af})} \right) \end{bmatrix}_{\tan^{-1} \theta \in [-90^\circ, 90^\circ]} \end{aligned} \quad (32)$$

where θ_x is phase angle of load voltage V_x which can be obtained by using phase-lock loop. By comparing the α_x with $\phi V_{xf} - V_{nf}$, the trigger signals to control thyristors can be obtained.

B. Active Inverter Part Control

For the active inverter part control, the modified synchronous reference frame method: instantaneous active and reactive current $i_d - i_q$ method [22] is implemented to improve the current harmonic compensation performance. Specifically, the active inverter part is generating the compensating current i_{cx} to track its reference value i_{cx}^* by using current hysteresis PWM control due to its simplicity of implementation, fast dynamic response, and good current-limiting capability. And the reference i_{cx}^* can be calculated as follows:

$$\begin{bmatrix} i_{ca}^* \\ i_{cb}^* \\ i_{cc}^* \end{bmatrix} = \sqrt{\frac{2}{3}} \cdot \begin{bmatrix} 1 & 0 \\ -1/2 & \sqrt{3}/2 \\ -1/2 & -\sqrt{3}/2 \end{bmatrix} \cdot \begin{bmatrix} \cos \theta_a & -\sin \theta_a \\ \sin \theta_a & \cos \theta_a \end{bmatrix} \cdot \begin{bmatrix} \tilde{i}_d \\ \tilde{i}_q \end{bmatrix} \quad (33)$$

where i_d and i_q are the instantaneous active and reactive current, which contain both dc components and ac components. The ac component \tilde{i}_d is obtained by passing i_d through a high-pass filter. And i_d and i_q can be obtained as follows:

$$\begin{bmatrix} i_d \\ i_q \end{bmatrix} = \begin{bmatrix} \cos \theta_a & \sin \theta_a \\ -\sin \theta_a & \cos \theta_a \end{bmatrix} \cdot \begin{bmatrix} i_\alpha \\ i_\beta \end{bmatrix}. \quad (34)$$

In (34), i_α and i_β in $\alpha\beta$ plane are transformed from abc plane as follows:

$$\begin{bmatrix} i_\alpha \\ i_\beta \end{bmatrix} = \begin{bmatrix} 1 & -1/2 & -1/2 \\ 0 & \sqrt{3}/2 & -\sqrt{3}/2 \end{bmatrix} \cdot \begin{bmatrix} i_{La} \\ i_{Lb} \\ i_{Lc} \end{bmatrix} \quad (35)$$

where i_{Lx} is the phase load current.

TABLE III
PARAMETER DESIGN FOR (A) UNBALANCED INDUCTIVE LOADS COMPENSATION

| | Conventional method [18] | Proposed method |
|-------------------------|---|---|
| Required X_{xf} | $X_{af} = -28.0,$ $X_{bf} = -41.6,$ $X_{cf} = -25.7$ (37) | $X_{af} = -27.2, X_{bf} = -50.5, X_{cf} = -20.9$ (11) |
| C_{PF} design by (18) | $[107, 74, 116 \mu\text{F}]_{\max} \leq C_{PF} \leq 2026 \mu\text{F}$ | $[111, 61, 141 \mu\text{F}]_{\max} \leq C_{PF} \leq 2026 \mu\text{F}$ |
| L_{PF} design by (16) | $L_{PF} \leq [94, 137, 86 \text{mH}]_{\min}$ | $L_{PF} \leq [92, 165, 71 \text{mH}]_{\min}$ |

TABLE IV
PARAMETER DESIGN FOR (B) MIXED INDUCTIVE AND CAPACITIVE LOADS COMPENSATION

| | Conventional method [18] | Proposed method |
|-------------------------|--|---|
| Required X_{xf} | $X_{af} = -45.2,$ $X_{bf} = 49.4,$ $X_{cf} = -56.5$ (37) | $X_{af} = -36.3,$ $X_{bf} = -88.2,$ $X_{cf} = -23.2$ (11) |
| C_{PF} design by (18) | $[68, -67, 54 \mu\text{F}]_{\max} \leq C_{PF} \leq 2026 \mu\text{F}$ | $[84, -36, 129 \mu\text{F}]_{\max} \leq C_{PF} \leq 2026 \mu\text{F}$ |
| L_{PF} design by (22) | $L_{PF} \leq P[156, 54, 195 \text{mH}]_{\min}$ | $L_{PF} \leq [134, 52, 324 \text{mH}]_{\min}$ |

V. SIMULATION CASE STUDIES

In this section, simulation case studies are provided to verify the proposed parameter design method for TCLC-HAPF which can perform full compensation under different unbalanced loading, while the TCLC-HAPF with the conventional design method [18] cannot always perform full compensation.

Two sets of testing loads are constructed for compensations namely: 1) unbalanced inductive loads; and 2) mixed inductive and capacitive loads. Referred to Fig. 2(a), with the $\bar{V}_x = 110 \text{ V}$, the active and reactive powers of two sets of testing loads are given as follows:

$$\begin{bmatrix} P_{La} + jQ_{La} \\ P_{Lb} + jQ_{Lb} \\ P_{Lc} + jQ_{Lc} \end{bmatrix} = \begin{bmatrix} 435 + j432 \\ 571 + j291 \\ 629 + j470 \end{bmatrix} \quad (36.a)$$

$$\begin{bmatrix} P_{La} + jQ_{La} \\ P_{Lb} + jQ_{Lb} \\ P_{Lc} + jQ_{Lc} \end{bmatrix} = \begin{bmatrix} 185 + j268 \\ 425 - j245 \\ 745 + j214 \end{bmatrix}. \quad (36.b)$$

Through the conventional parameter design method [18], X_{xf} calculated by conventional method is expressed as follows:

$$\begin{bmatrix} X_{af} \\ X_{bf} \\ X_{cf} \end{bmatrix} = \begin{bmatrix} \bar{V}_x^2 / Q_{La} \\ \bar{V}_x^2 / Q_{Lb} \\ \bar{V}_x^2 / Q_{Lc} \end{bmatrix}. \quad (37)$$

Based on load power given in (36.a) and (36.b), the parameter design procedures of the conventional [18] and proposed methods are summarized in Tables III and IV.

TABLE V
DESIGN OF TCLC-HAPF BY APPLYING THE CONVENTIONAL AND PROPOSED DESIGN METHODS

| | C_{PF} | L_{PF} | V_{DC} (28) | L_c (29) |
|---------------------|-------------|----------|---------------|------------|
| Conventional method | 120 μF | 30 mH | 60 V | 5 mH |
| Proposed method | 160 μF | 30 mH | 60 V | 5 mH |

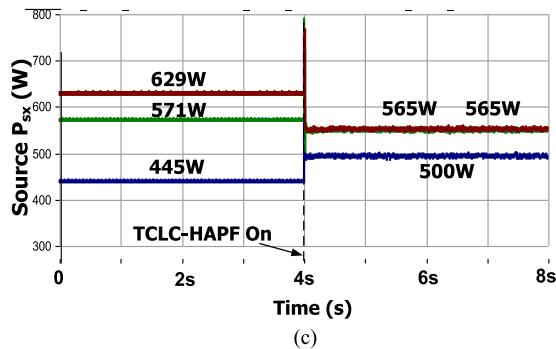
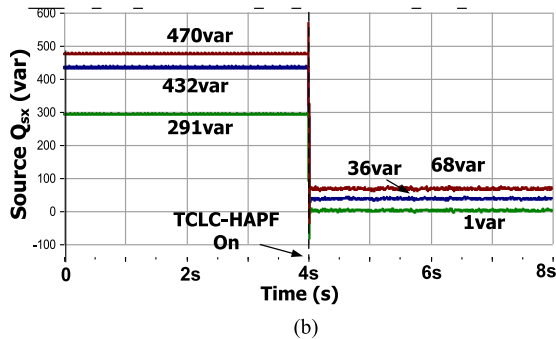
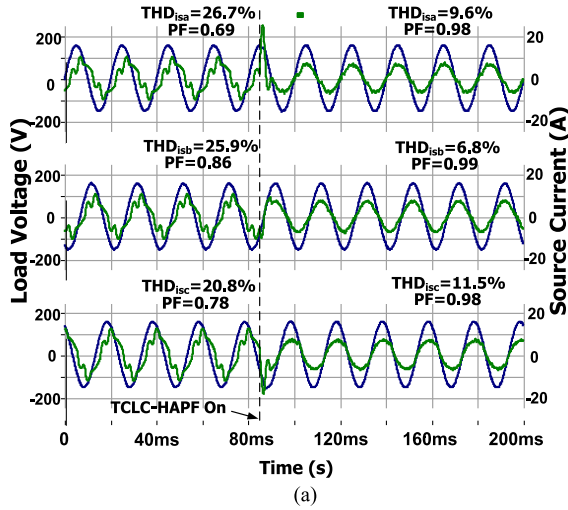


Fig. 5. Dynamic performance by using TCLC-HAPF with conventional design method [18] for unbalanced inductive loads compensation: (a) v_{sx} and i_{sx} , (b) Q_{sx} , and (c) P_{sx} .

To obtain the parameter values in **Table V**, the following three conditions are required to be satisfied simultaneously.

- 1) Since TCLC-HAPF aims to compensate both unbalanced inductive loads and mixed inductive and capacitive loads, their corresponding design values (C_{PF} and L_{PF}) should

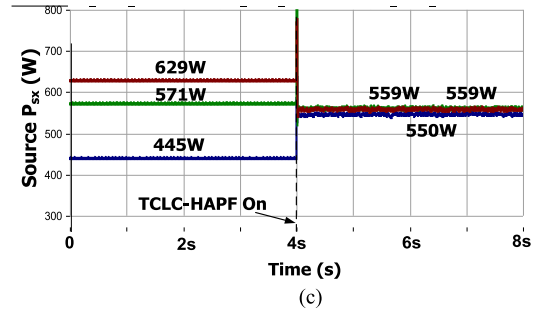
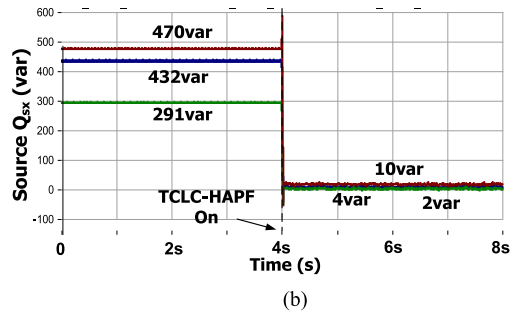
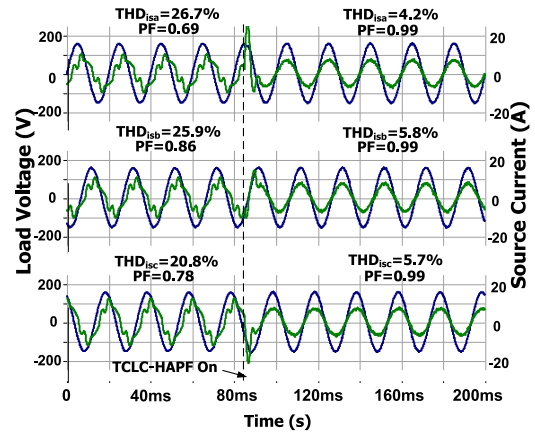
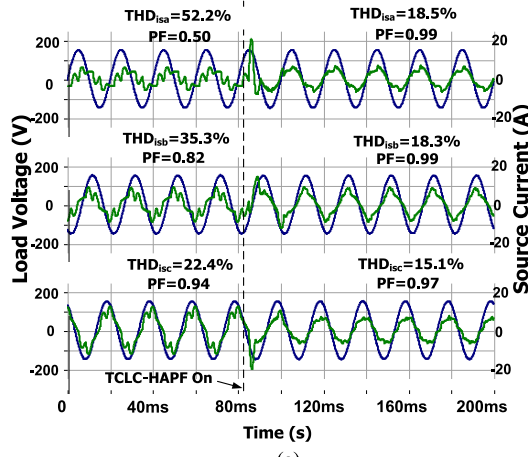


Fig. 6. Dynamic performance by using TCLC-HAPF with the proposed design method for unbalanced inductive loads compensation: (a) v_{sx} and i_{sx} , (b) Q_{sx} , and (c) P_{sx} .

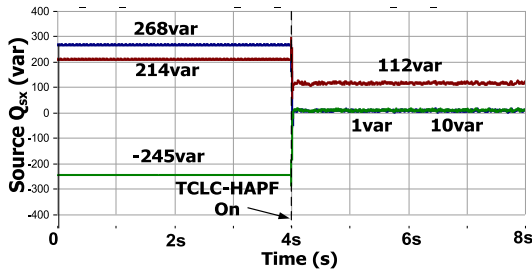
satisfy the conditions listed in **Tables II** and **III** simultaneously.

- 2) To prove the conventional method may provide insufficient compensation range, the conventionally designed C_{PF} should be within the range calculated by the conventional method and outside of the range calculated by the proposed method simultaneously.
- 3) The designed component values should be the commonly used experimental component values in the laboratory.

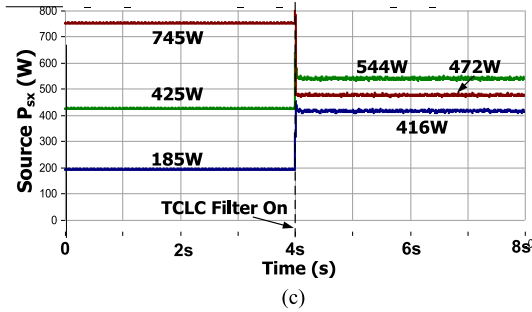
By satisfying the previous conditions, the final selected C_{PF} value using the conventional method is 120 μF (two parallel-connected CCB65-AC450V-60 μF capacitors), and the final selected C_{PF} value using the proposed method is 160 μF (two parallel connected CCB65-AC450V-80 μF capacitors). Following the same design process of C_{PF} , L_{PF} is selected as 30 mH. Besides, according to the constructed loading harmonic current ($I_{L_{Xn}}$) in Sections IV and V, V_{DC} is designed to be



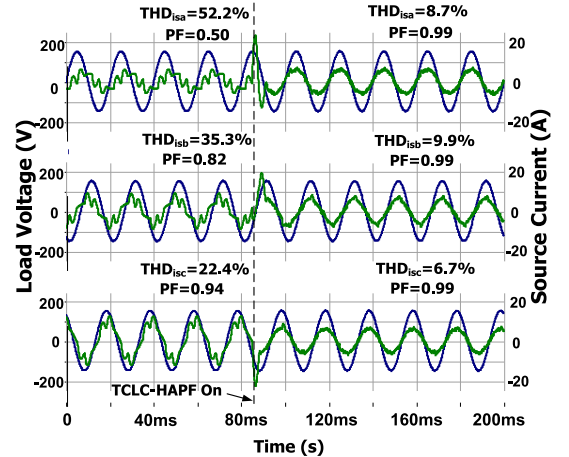
(a)



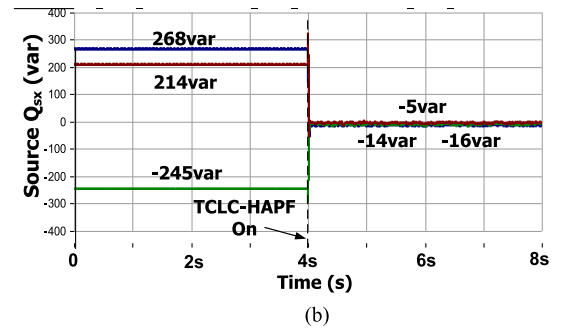
(b)



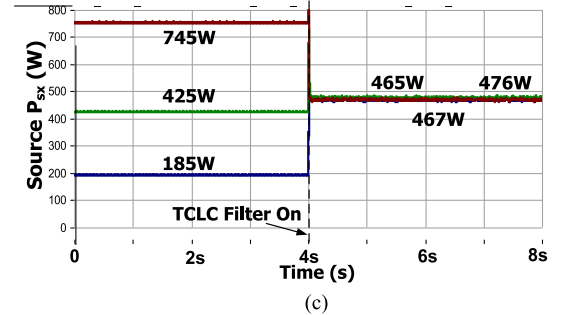
(c)



(a)



(b)



(c)

Fig. 7. Dynamic performance by using TCLC-HAPF with the conventional design method [18] for mixed inductive and capacitive loads compensation: (a) v_{sx} and i_{sx} , (b) Q_{sx} , and (c) P_{sx} .

60 V (28), which is sufficient for compensations. Also, according to simulation and experimental settings ($f_s = 5$ kHz and $\Delta i_{Lcmax} = 0.4$ A), L_c is designed to be 5 mH, which can satisfy (29) (>3.75 mH).

To compensate the two sets of testing loads as shown in (36.a) and (36.b), the TCLC-HAPF designed by the conventional method [18] and the proposed method are applied. Figs. 5–8 show the simulation compensation results of source voltages (v_{sx}) and currents (i_{sx}), source reactive (Q_{sx}) and active power (P_{sx}) before and after TCLC-HAPF compensation. Figs. 8 and 9 show phasor diagrams of source voltages and currents. Table VI summarizes the simulated compensation results. In this paper, with referenced to the IEEE standard 519-2014 [23], the current THD_{isx} is required to be lower than 15% under conditions of $I_{Sc}/I_L \in [100, 1000]$ (this laboratory-scaled setup) and $THD_{isx} = TDD_{isx} = 15\%$ at the worst case analysis [18].

Fig. 8. Dynamic performance by using TCLC-HAPF with the proposed design method for mixed inductive and capacitive loads compensation: (a) v_{sx} and i_{sx} , (b) Q_{sx} , and (c) P_{sx} .

After the TCLC-HAPF compensation with the conventional design method, the fundamental source reactive power of phases *a* and *c* (unbalanced inductive loads in Fig. 5) and phase *c* (mixed inductive and capacitive loads in Fig. 7) cannot be compensated to be close to zero, and the fundamental source active powers are not balanced for both loadings cases. The source voltage and current are not all in phase with each other after compensations as shown in Figs. 9 and 10. From Figs. 5(a) and 7(a) and Table VI, the worst phase source current total harmonic distortions (THD_{isx}) after TCLC-HAPF (by the conventional method) compensation are 11.5% for unbalanced inductive loads case, and 18.5% for mixed inductive and capacitive loads case, in which the compensated $THD_{isx} = 18.5\%$ does not satisfy the IEEE standard ($THD < 15\%$) [23]. The source current unbalanced factor (UBI_{fs}) is 12.0% for unbalanced inductive

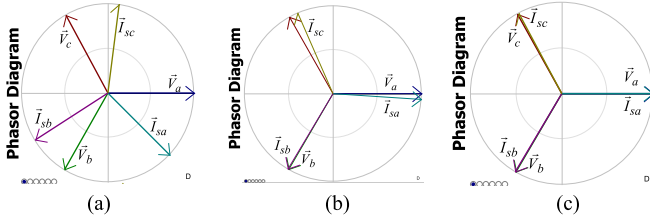


Fig. 9. Simulated phasor diagrams of v_{sx} and i_{sx} for unbalanced inductive loads compensation: (a) before compensation, (b) after TCLC-HAPF (by the conventional method [18]) compensation, and (c) after TCLC-HAPF (by the proposed design method) compensation.

TABLE VI

SIMULATION RESULTS FOR UNBALANCED LOADS COMPENSATION BEFORE AND AFTER TCLC-HAPF COMPENSATION

| | | Q_{sx} (var) | P_{sx} (W) | PF | i_{sx} (A) | THD_{isx} (%) | UBI_{fs} (%) | V_{DC} (V) | |
|------------------------------------|------------------------------------|-------------------|-----------------|------|-----------------|--------------------|-------------------|-----------------|----|
| Unbalanced Inductive loads | Before Comp. | A | 432 | 445 | 0.69 | 5.6 | 26.7 | 25.8 | - |
| | | B | 291 | 571 | 0.86 | 5.8 | 25.9 | | |
| | | C | 470 | 629 | 0.78 | 7.2 | 20.8 | | |
| | TCLC-HAPF (Conventional method) | A | 36 | 500 | 0.98 | 4.5 | 9.6 | 12.0 | 60 |
| | | B | 1 | 565 | 0.99 | 5.1 | 6.8 | | |
| | | C | 68 | 565 | 0.98 | 5.1 | 11.5 | | |
| | TCLC-HAPF (Proposed method) | A | 4 | 550 | 0.99 | 4.8 | 4.2 | 2.0 | 60 |
| | | B | 2 | 559 | 0.99 | 4.9 | 5.8 | | |
| | | C | 10 | 559 | 0.99 | 4.9 | 5.7 | | |
| Mixed Inductive & Capacitive loads | Before Comp. | A | 268 | 185 | 0.50 | 3.1 | 52.2 | 76.5 | - |
| | | B | -245 | 425 | 0.82 | 4.6 | 35.3 | | |
| | | C | 214 | 745 | 0.94 | 6.8 | 22.4 | | |
| | TCLC-HAPF (Conventional method) | A | 1 | 416 | 0.99 | 4.0 | 18.5 | 24.1 | 60 |
| | | B | 10 | 544 | 0.99 | 5.1 | 18.3 | | |
| | | C | 112 | 472 | 0.97 | 4.6 | 15.1 | | |
| | TCLC-HAPF (Proposed method) | A | -5 | 465 | 0.99 | 4.4 | 8.7 | 2.2 | 60 |
| | | B | -14 | 476 | 0.99 | 4.5 | 9.9 | | |
| | | C | -16 | 467 | 0.99 | 4.5 | 6.7 | | |

*Notes the shades areas mean undesirable results.

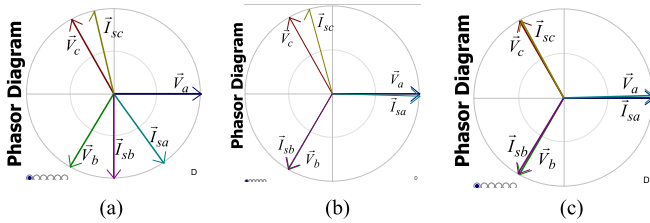


Fig. 10. Simulated phasor diagrams of v_{sx} and i_{sx} for mixed inductive and capacitive loads compensation: (a) before compensation, (b) after TCLC-HAPF (by the conventional method [18]) compensation, and (c) after TCLC-HAPF (by the proposed design method) compensation.

loads compensation and 24.1% for mixed inductive and capacitive loads compensation, respectively.

With the proposed parameter design method, the TCLC-HAPF can balance the three-phase active power and compensate the reactive power for both loading cases as shown in Figs. 6 and 8 and Table VI. As shown in Figs. 8 and 9, the source voltage and current are in phase with each other after TCLC-HAPF compensation. Moreover, the THD_{isx} has been reduced to less than 6% for unbalanced inductive loading compensation and 10% for mixed inductive and capacitive loading compensation, which can satisfy the IEEE standard [23]. In Table VI,



Fig. 11. Experimental setup of the 110 V-5 kV-A TCLC-HAPF experimental prototype.

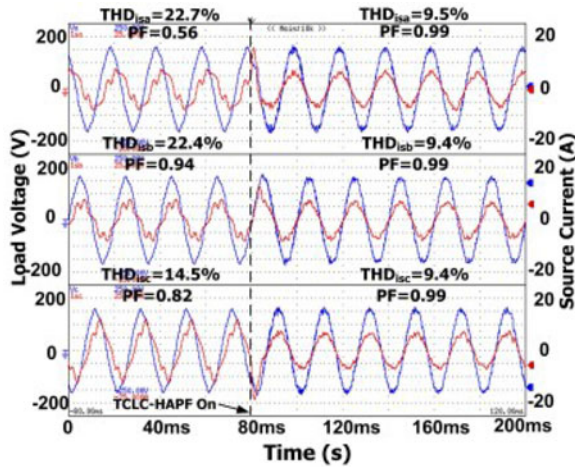
it is shown that the source current unbalanced factor (UBI_{fs}) is less than 3.0% after compensation by TCLC-HAPF with the proposed design method.

VI. EXPERIMENTAL RESULTS AND DISCUSSIONS

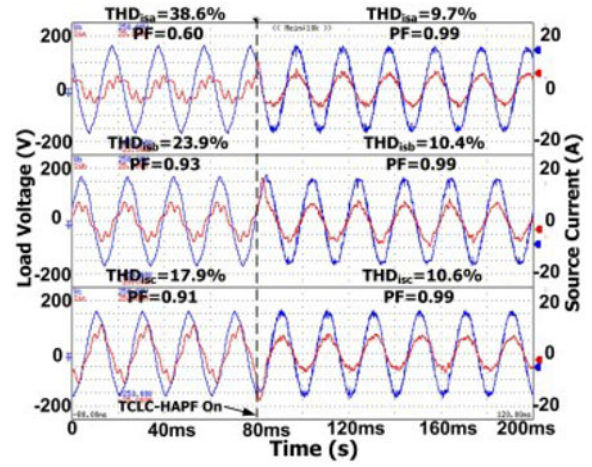
A. Experimental Results

In this section, a 110 V-5 kV-A experimental prototype of TCLC-HAPF with the proposed design method is built in laboratory as shown in Fig. 11. The digital control system of the TCLC-HAPF is digital signal processor TMS320F2812, and the sampling frequency of the control system is 25 kHz. The switching devices for the inverter are Mitsubishi IGBT intelligent power modules PM300DSA060. And the switching devices for the TCLC are thyristors SanRex PK110FG160. Moreover, the experimental parameters of the TCLC-HAPF and the test loadings are basically the same as the above simulation in Table V and (36.a) and (36.b).

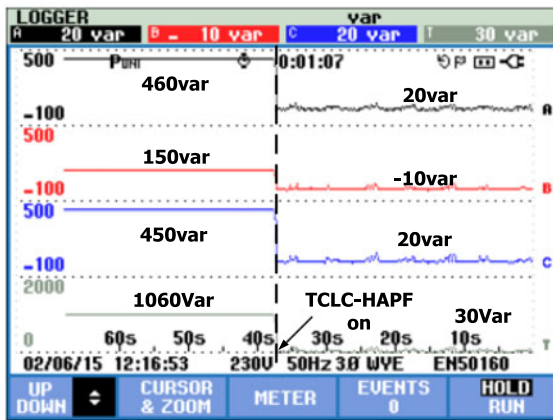
From Figs. 12(a) and 13(a), after TCLC-HAPF compensation, the worst phase PF has been compensated from original 0.56 for unbalanced inductive loads and 0.60 for mixed inductive and capacitive loads to 0.99. The worst phase THD_{isx} have been compensated to 9.5% and 10.6% from the original 22.7% for unbalanced inductive loads and 38.6% for mixed inductive and capacitive loads, which can meet the IEEE standard ($THD < 15\%$) [23]. From Figs. 12 and 13(b) and (c) and Table VII, with the proposed parameter design method, the TCLC-HAPF can compensate the fundamental reactive power from 460, 150, and 450 var for unbalanced inductive loads and 260, -150, and 290 var for mixed loads to almost zero. Also, the proposed TCLC-HAPF can balance the fundamental active power from 310, 520, and 600 W to about 530 W for unbalanced inductive loads and from 230, 510, and 680 W to about 500 W for mixed loads. As shown in Fig. 14, the source voltage and current are in phase with each other after TCLC-HAPF compensation. Moreover, the UBI_{fs} is less than 5.0% after compensation from the original 43.1% and 54.3% for two sets of loading.



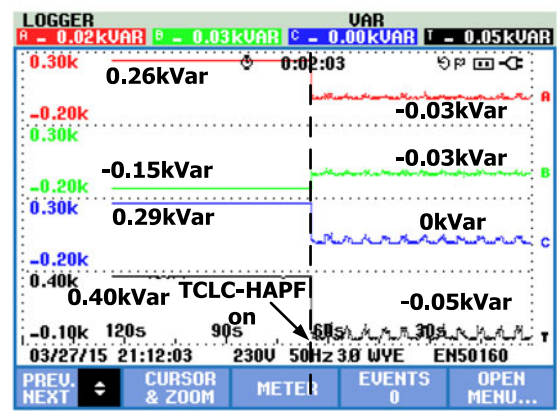
(a)



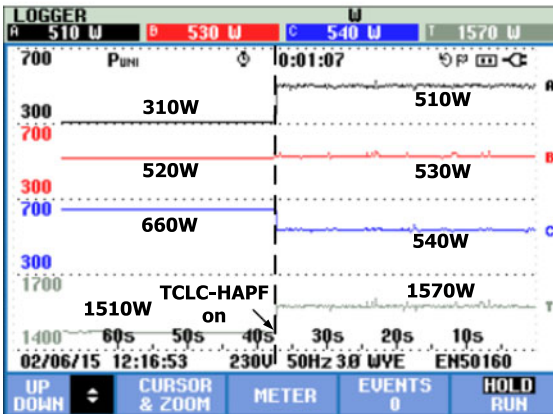
(a)



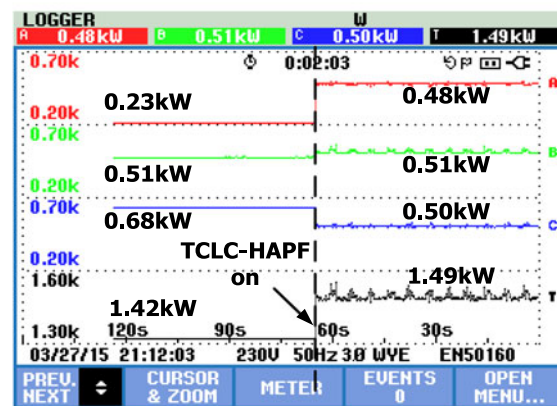
(b)



(b)



(c)



(c)

Fig. 12. Dynamic unbalanced inductive loads compensation by using TCLC-HAPF with the proposed design: (a) v_{sx} and i_{sx} , (b) Q_{sx} , and (c) P_{sx} .

Fig. 13. Dynamic mixed inductive and capacitive loads compensation by using TCLC-HAPF with the proposed design: (a) v_{sx} and i_{sx} , (b) Q_{sx} , and (c) P_{sx} .

B. Discussions and Error Analysis

The experimental results as in Figs. 12–14 and Table VII are consistent with the simulation results as in Figs. 6, 8–10, and Table VI, which verifies that the proposed TCLC-HAPF modeling and parameter design method can achieve superior compensating performance for unbalanced compensation when compared with the conventional design method [18]. Table VIII

shows the comparison between the conventional TCLC-HAPF parameter design method and the proposed one.

However, comparing Tables VII and VI, there are differences between simulation and experimental results, which are actually due to the equivalent series resistance in hardware components, the difference of the resolution of the transducers, the digital computation error and the noise in the experiment. Also, these

TABLE VII

EXPERIMENTAL RESULTS FOR UNBALANCED LOADS COMPENSATION BEFORE AND AFTER TCLC-HAPF COMPENSATION

| | | | Q_{sx} (var) | P_{sx} (W) | PF | i_{sx} (A) | THD _{isx} (%) | UBI _{f5} (%) | V_{DC} (V) |
|---|-----------------------------------|---|-------------------|-----------------|------|-----------------|---------------------------|--------------------------|-----------------|
| Unbalanced Inductive Loads | Before Comp. | A | 460 | 310 | 0.56 | 5.1 | 22.7 | 43.1 | -- |
| | | B | 150 | 520 | 0.94 | 4.9 | 22.4 | | |
| | | C | 450 | 600 | 0.82 | 7.4 | 14.5 | | |
| | TCLC-HAPF (Proposed method) | A | 20 | 510 | 0.99 | 4.6 | 9.5 | 4.3 | 60 |
| | | B | -10 | 530 | 0.99 | 4.6 | 9.4 | | |
| | | C | 20 | 540 | 0.99 | 4.8 | 9.4 | | |
| Mixed Inductive & Capacitive loads | Before Comp. | A | 260 | 230 | 0.60 | 3.1 | 38.6 | 54.3 | -- |
| | | B | -150 | 510 | 0.93 | 4.6 | 23.9 | | |
| | | C | 290 | 680 | 0.91 | 6.8 | 17.9 | | |
| | TCLC-HAPF (Proposed method) | A | -30 | 480 | 0.99 | 4.5 | 9.7 | 2.2 | 60 |
| | | B | -30 | 510 | 0.99 | 4.5 | 10.4 | | |
| | | C | 0 | 500 | 0.99 | 4.6 | 10.6 | | |

*Notes the shades areas mean undesirable results.

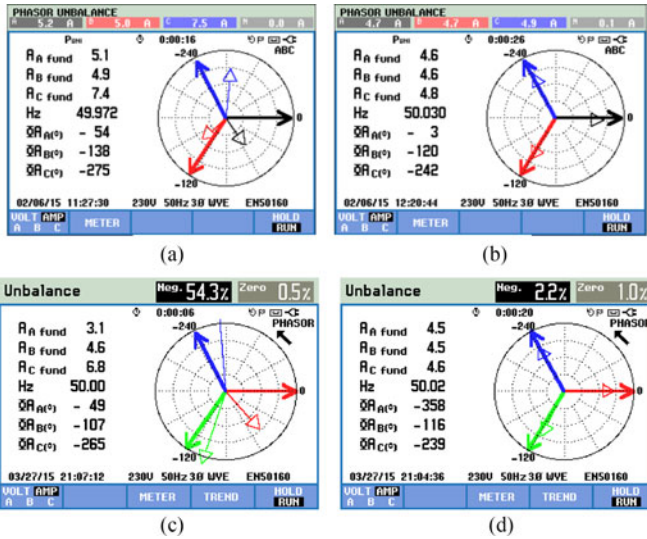


Fig. 14. Experimental phasor diagrams of v_{sx} and i_{sx} compensation: (a) before compensation for unbalanced inductive loads, (b) after TCLC-HAPF compensation for unbalanced inductive loads, (c) before compensation for mixed inductive and capacitive loads, and (d) after TCLC-HAPF compensation for mixed inductive and capacitive loads.

TABLE VIII

COMPARISON BETWEEN THE CONVENTIONAL TCLC-HAPF PARAMETER DESIGN METHOD [18] AND THE PROPOSED ONE

| Modeling | TCLC part design | Advantages | Disadvantages |
|------------------------------------|---------------------------------|--|--|
| Conventional TCLC-HAPF design [18] | Single-phase modeling | Max. phase of premeasured Q_{Lx} | Smaller parameter values Insufficient compensation range/poor performance |
| Proposed TCLC-HAPF design | Unbalanced three-phase modeling | Inner flow unbalanced power and max. phase of premeasured Q_{Lx} | Sufficient compensation range/good performance Slightly larger component values |

TABLE IX

COMPARISON BETWEEN THE CONVENTIONAL METHOD [18] AND THE PROPOSED METHOD

| Conventional method [18] | Proposed method |
|---|---|
| Circuit model in Fig.3 of [18] | Circuit model in Fig.2(a) in this paper |
| Calculate the TCLC fundamental impedance X_{cf} based on (37) and (11) with target $X_{Acxf} \approx 0$ | |
| $\begin{bmatrix} X_{cf} \\ X_{bf} \\ X_{cf} \end{bmatrix} = \begin{bmatrix} \bar{V}_x^2 / Q_{La} \\ \bar{V}_x^2 / Q_{Lb} \\ \bar{V}_x^2 / Q_{Lc} \end{bmatrix} = \begin{bmatrix} -28.0 \\ -41.6 \\ -27.7 \end{bmatrix}$ | $\begin{bmatrix} X_{af} \\ X_{bf} \\ X_{cf} \end{bmatrix} = \begin{bmatrix} \frac{3\bar{V}_x^2(Q_{La}-Q_{Lb}-Q_{Lc}) + (Q_{La}-Q_{Lb}-Q_{Lc})\bar{V}_x^2}{(Q_{La}-Q_{Lb}-Q_{Lc})\bar{V}_x^2 + (Q_{La}-Q_{Lb}-Q_{Lc})\bar{V}_x^2} \\ \frac{3\bar{V}_x^2(Q_{La}-Q_{Lb}-Q_{Lc}) + (Q_{La}-Q_{Lb}-Q_{Lc})\bar{V}_x^2}{(Q_{La}-Q_{Lb}-Q_{Lc})\bar{V}_x^2 + (Q_{La}-Q_{Lb}-Q_{Lc})\bar{V}_x^2} \\ \frac{3\bar{V}_x^2(Q_{La}-Q_{Lb}-Q_{Lc}) + (Q_{La}-Q_{Lb}-Q_{Lc})\bar{V}_x^2}{(Q_{La}-Q_{Lb}-Q_{Lc})\bar{V}_x^2 + (Q_{La}-Q_{Lb}-Q_{Lc})\bar{V}_x^2} \end{bmatrix}$ $= \begin{bmatrix} -27.2 \\ -50.6 \\ -20.9 \end{bmatrix}$ |
| Calculate the fundamental compensating current \bar{I}_{cf} | |
| $\begin{bmatrix} \bar{I}_{caf} \\ \bar{I}_{cbf} \\ \bar{I}_{ccf} \end{bmatrix} = \begin{bmatrix} \bar{V}_a / jX_{af} \\ \bar{V}_b / jX_{bf} \\ \bar{V}_c / jX_{cf} \end{bmatrix} = \begin{bmatrix} 3.9 \angle 90.0^\circ \\ 2.7 \angle -30.0^\circ \\ 4.3 \angle -150.0^\circ \end{bmatrix}$ | $\begin{bmatrix} \bar{I}_{caf} \\ \bar{I}_{cbf} \\ \bar{I}_{ccf} \end{bmatrix} = \begin{bmatrix} (\bar{V}_a - \bar{V}_{nf}) / jX_{af} \\ (\bar{V}_b - \bar{V}_{nf}) / jX_{bf} \\ (\bar{V}_c - \bar{V}_{nf}) / jX_{cf} \end{bmatrix} = \begin{bmatrix} 4.0 \angle 76.2^\circ \\ 2.7 \angle -25.2^\circ \\ 4.4 \angle -140.8^\circ \end{bmatrix}$ <p>where</p> $\bar{V}_{nf} = \frac{X_{bf} \cdot X_{cf}}{X_{af} X_{bf} + X_{bf} X_{cf} + X_{cf} X_{af}} \bar{V}_a + \frac{X_{cf} \cdot X_{af}}{X_{af} X_{bf} + X_{bf} X_{cf} + X_{cf} X_{af}} \bar{V}_b + \frac{X_{af} \cdot X_{bf}}{X_{af} X_{bf} + X_{bf} X_{cf} + X_{cf} X_{af}} \bar{V}_c$ |
| Calculate the source current \bar{I}_{sx} | |
| $\begin{bmatrix} \bar{I}_{saf} \\ \bar{I}_{sbf} \\ \bar{I}_{scf} \end{bmatrix} = \begin{bmatrix} \bar{I}_{Laf} \\ \bar{I}_{Lbf} \\ \bar{I}_{Lcf} \end{bmatrix} + \begin{bmatrix} \bar{I}_{caf} \\ \bar{I}_{cbf} \\ \bar{I}_{ccf} \end{bmatrix} = \begin{bmatrix} 4.0 \angle 0^\circ \\ 5.2 \angle -120^\circ \\ 5.7 \angle 120^\circ \end{bmatrix}$ | $\begin{bmatrix} \bar{I}_{saf} \\ \bar{I}_{sbf} \\ \bar{I}_{scf} \end{bmatrix} = \begin{bmatrix} \bar{I}_{Laf} \\ \bar{I}_{Lbf} \\ \bar{I}_{Lcf} \end{bmatrix} + \begin{bmatrix} \bar{I}_{caf} \\ \bar{I}_{cbf} \\ \bar{I}_{ccf} \end{bmatrix} = \begin{bmatrix} 5.0 \angle 0^\circ \\ 5.0 \angle -120^\circ \\ 5.0 \angle 120^\circ \end{bmatrix}$ |
| Calculate the active power and reactive power in source side | |
| $\begin{bmatrix} P_{sa} + jQ_{sa} \\ P_{sb} + jQ_{sb} \\ P_{sc} + jQ_{sc} \end{bmatrix} = \begin{bmatrix} \bar{V}_a \bar{I}_{saf}^* \\ \bar{V}_b \bar{I}_{sbf}^* \\ \bar{V}_c \bar{I}_{scf}^* \end{bmatrix} = \begin{bmatrix} 440 + j0 \\ 572 + j0 \\ 627 + j0 \end{bmatrix}$ | $\begin{bmatrix} P_{sa} + jQ_{sa} \\ P_{sb} + jQ_{sb} \\ P_{sc} + jQ_{sc} \end{bmatrix} = \begin{bmatrix} \bar{V}_a \bar{I}_{saf}^* \\ \bar{V}_b \bar{I}_{sbf}^* \\ \bar{V}_c \bar{I}_{scf}^* \end{bmatrix} = \begin{bmatrix} 550 + j0 \\ 550 + j0 \\ 550 + j0 \end{bmatrix}$ |

factors can affect the TCLC-HAPF compensation performances in experimental results.

VII. CONCLUSION

In this paper, a three-phase modeling of TCLC-HAPF for unbalanced compensation was proposed instead of using the conventional equivalent single-phase modeling. Based on the above proposed modeling, the parameter design method for TCLC-HAPF was proposed considering inner flowed unbalanced power among each phase in order to obtain a sufficient compensation range. To prove the advantages of the proposed method over the conventional one in Table VIII, representative simulation and experimental results were given. It is proved that the TCLC-HAPF can balance the source active power, compensate loading reactive power and harmonic currents, while the conventional parameter design method cannot achieve satisfactory compensation due to its insufficient compensation range design.

APPENDIX

A. Comparison Between the Conventional and Proposed Modeling Methods

A case study is provided to prove the advantage of the proposed modeling method over the conventional one [18]. Referring to Fig. 1, the unbalanced phase load apparent powers are

assumed to be

$$\begin{bmatrix} P_{La} + jQ_{La} \\ P_{Lb} + jQ_{Lb} \\ P_{Lc} + jQ_{Lc} \end{bmatrix} = \begin{bmatrix} 435 + j432 \\ 571 + j291 \\ 629 + j470 \end{bmatrix}. \quad (38)$$

The phase load currents \vec{I}_{Lxf} can be calculated as follows:

$$\begin{bmatrix} \vec{I}_{Laf} \\ \vec{I}_{Lbf} \\ \vec{I}_{Lcf} \end{bmatrix} = \begin{bmatrix} \left[\frac{(P_{La} + jQ_{La})}{\vec{V}_a} \right]^* \\ \left[\frac{(P_{Lb} + jQ_{Lb})}{\vec{V}_b} \right]^* \\ \left[\frac{(P_{Lc} + jQ_{Lc})}{\vec{V}_c} \right]^* \end{bmatrix} = \begin{bmatrix} 5.57 \angle -44.8^\circ \\ 5.82 \angle -147.0^\circ \\ 7.13 \angle 83.2^\circ \end{bmatrix} \quad (39)$$

where the rms value of load voltage is given as: $\bar{V}_x = 110$ V, where $\vec{V}_a = \bar{V}_x \angle 0^\circ$, $\vec{V}_b = \bar{V}_x \angle -120^\circ$, and $\vec{V}_c = \bar{V}_x \angle 120^\circ$. The comparison between the conventional method [18] and the proposed method are shown in Table IX.

Based on previous comparison, it can be shown that the conventional method can compensate Q_{sx} while it cannot balance P_{sx} ($P_{sa} \neq P_{sb} \neq P_{sc}$ and $Q_{sa} = Q_{sb} = Q_{sc} = 0$). On the other hand, the proposed method can balance P_{sx} and compensate Q_{sx} ($P_{sa} = P_{sb} = P_{sc}$ and $Q_{sa} = Q_{sb} = Q_{sc} = 0$). The proposed modeling has also been verified by simulation (see Figs. 6, 8–10 and Table VI) and experimental results (see Figs. 12–14 and Table VII).

REFERENCES

- [1] V. Trujillo, C. R. Fuerte-Esquivel, and J. H. Tovar Hernandez, "Advanced three-phase static VAR compensator models for power flow analysis," *Proc. IEE—Gener., Transmiss. Distrib.*, vol. 150, no. 1, pp. 119–126, Jan. 2003.
- [2] J.-H. Chen, W.-J. Lee, and M.-S. Chen, "Using a static VAR compensator to balance a distribution system," *IEEE Trans. Ind. Appl.*, vol. 35, no. 2, pp. 298–304, Mar./Apr. 1999.
- [3] W.-N. Chang and C.-J. Wu, "Developing static reactive power compensators in a power system simulator for power education," *IEEE Trans. Power Syst.*, vol. 10, no. 4, pp. 1734–1741, Nov. 1995.
- [4] A. Hamadi, S. Rahmani, and K. Al-Haddad, "A hybrid passive filter configuration for VAR control and harmonic compensation," *IEEE Trans. Ind. Electron.*, vol. 57, no. 7, pp. 2419–2434, Jul. 2010.
- [5] L. Wang, C.-S. Lam, and M. C. Wong, "Design of a thyristor controlled LC compensator for dynamic reactive power compensation in smart grid," *IEEE Trans. Smart Grid*, to be published, doi: 10.1109/TSG.2016.2578178.
- [6] H. Nian, Y. Shen, H. Yang, and Y. Quan, "Flexible grid connection technique of voltage-source inverter under unbalanced grid conditions based on direct power control," *IEEE Trans. Ind. Appl.* vol. 51, no. 5, pp. 4041–4050, Sep./Oct. 2015.
- [7] P. R. Martinez-Rodriguez, G. Escobar, A. A. Valdez-Fernandez, M. Hernandez-Gomez, and J. M. Sosa, "Direct power control of a three phase rectifier based on positive sequence detection," *IEEE Trans. Ind. Electron.*, vol. 61, no. 8, pp. 4084–4092, Aug. 2014.
- [8] Z.-X. Zou, K. Zhou, Z. Wang, and M. Cheng, "Frequency-adaptive fractional-order repetitive control of shunt active power filters," *IEEE Trans. Ind. Electron.*, vol. 62, no. 3, pp. 1659–1668, Mar. 2015.
- [9] M. Qasim, P. Kanjiya, and V. Khadkikar, "Artificial-neural-network-based phase-locking scheme for active power filters," *IEEE Trans. Ind. Electron.*, vol. 61, no. 8, pp. 3857–3866, Aug. 2014.
- [10] H. Hu and Y. Xing, "Design considerations and fully digital implementation of 400-Hz active power filter for aircraft applications," *IEEE Trans. Ind. Electron.*, vol. 61, no. 8, pp. 3823–3834, Aug. 2014.
- [11] L. Wang, C.-S. Lam, and M.-C. Wong, "An adaptive hysteresis band controller for LC-coupling hybrid active power filter with approximate constant switching frequency," in *Proc. IEEE PES Asia-Pacific Power Energy Eng. Conf.*, Hong Kong, 2014, pp. 1–5.
- [12] L. Wang, C. S. Lam, M. C. Wong, N. Y. Dai, K. W. Lao, and C. K. Wong, "Non-linear adaptive hysteresis band pulse-width modulation control for hybrid active power filters to reduce switching loss," *IET Power Electron.*, vol. 8, no. 11, pp. 2156–2167, Nov. 2015.
- [13] K.-W. Lao, M.-C. Wong, N. Y. Dai, C.-S. Lam, C.-K. Wong, and L. Wang, "Analysis in the effect of Co-phase traction railway HPQC coupled impedance on its compensation capability and impedance-mapping design technique based on required compensation capability for reduction in operation voltage," *IEEE Trans. Power Electron.*, to be published, doi: 10.1109/TPEL.2016.2575446.
- [14] J. Dixon, Y. del Valle M. Orchard, M. Ortuzar, L. Moran, and C. Maffrand, "A full compensating system for general loads, based on a combination of thyristor binary compensator, and a PWM-IGBT active power filter," *IEEE Trans. Ind. Electron.*, vol. 50, no. 5, pp. 982–989, Oct. 2003.
- [15] A. Luo, Z. Shuai, W. Zhu, and Z. J. Shen, "Combined system for harmonic suppression and reactive power compensation," *IEEE Trans. Ind. Electron.*, vol. 56, no. 2, pp. 418–428, Feb. 2009.
- [16] A. Luo, S. Peng, C. Wu, J. Wu, and Z. Shuai, "Power electronic hybrid system for load balancing compensation and frequency-selective harmonic suppression," *IEEE Trans. Ind. Electron.*, vol. 59, no. 2, pp. 723–732, Feb. 2012.
- [17] S. Rahmani, A. Hamadi, K. Al-Haddad, and L. A. Dessaint, "A combination of shunt hybrid power filter and thyristor-controlled reactor for power quality," *IEEE Trans. Ind. Electron.*, vol. 61, no. 5, pp. 2152–2164, May 2014.
- [18] L. Wang, C.-S. Lam, and M.-C. Wong, "A hybrid-STATCOM with wide compensation range and low dc-link voltage," *IEEE Trans. Ind. Electron.*, vol. 63, no. 6, pp. 3333–3343, Jun. 2016.
- [19] L. Wang, C.-S. Lam, and M.-C. Wong, "Hardware and software design of a low DC-link voltage and wide compensation range thyristor controlled LC-coupling hybrid active power filter," in *Proc. 2015 IEEE Region 10 Conf.*, Macao, China, 2015, pp. 1–4.
- [20] R. B. Gonzatti, S. C. Ferreira, C. H. da Silva, R. R. Pereira, L. E. Borges da Silva, and G. Lambert-Torres, "Smart impedance: A new way to look at hybrid filters," *IEEE Trans. Smart Grid*, vol. 7, no. 2, pp. 837–846, Mar. 2016.
- [21] C. H. da Silva *et al.*, "Smart impedance: Expanding the hybrid active series power filter concept," in *Proc. 38th Annu. Conf. IEEE Ind. Electron. Soc.*, Montreal, QC, Canada, 2012, pp. 1416–1421.
- [22] V. Soares, P. Verdelho, and G. D. Marques, "An instantaneous active and reactive current component method for active filters," *IEEE Trans. Power Electron.*, vol. 15, no. 4, pp. 660–669, Jul. 2000.
- [23] *IEEE Recommended Practices and Requirements for Harmonic Control in Electrical Power Systems*, IEEE Standard 519-2014, 2014.



Lei Wang received the B.Sc. degree in electrical and electronics engineering from the University of Macau (UM), Macao, China, in 2011, and the M.Sc. degree in electronics engineering from the Hong Kong University of Science and Technology, Hong Kong, China, in 2012. Since 2012, he has been working toward the Ph.D. degree in electrical and computer engineering in the Power Electronics Laboratory, UM.

His research interests include power electronics, power quality and distribution flexible ac transmission systems, power quality compensation, and renewable energy.

Mr. Wang received the Champion Award in the "Schneider Electric Energy Efficiency Cup" competition held in Hong Kong, in 2011.



Chi-Seng Lam (S'04–M'12–SM'16) received the B.Sc., M.Sc., and Ph.D. degrees in electrical and electronics engineering from the University of Macau (UM), Macao, China, in 2003, 2006, and 2012, respectively.

From 2006 to 2009, he was an Electrical and Mechanical Engineer with UM. From 2009 to 2012, he was a Laboratory Technician with UM. In 2013, he was a Postdoctoral Fellow with The Hong Kong Polytechnic University, Hong Kong, China. He is currently an Assistant Professor in

the State Key Laboratory of Analog and Mixed Signal VLSI, UM. He has coauthored two books and more than 50 technical journal and conference papers. His research interests include integrated controllers, power management integrated circuits, power quality compensators, smart grid technology, renewable energy, etc.

Dr. Lam is a Vice-Chair of the IEEE Macau Section. He received the Macao Science and Technology Invention Award (Third-Class) and R&D Award for the Ph.D. degree in 2014 and 2012, respectively, and the RIUPEEEEC Merit Paper Award in 2005.



Man-Chung Wong (SM'06) received the B.Sc. and M.Sc. degrees in electrical and electronics engineering from the University of Macau, Macao, China, in 1993 and 1997, respectively, and the Ph.D. degree in electrical engineering from Tsinghua University, Beijing, China, in 2003.

From July 2014 to December 2014, he was a Visiting Fellow at the University of Cambridge, Cambridge, U.K. He is currently an Associate Professor in the Department of Electrical and Computer Engineering, University of Macau. His research interests include power electronics converters, pulse width modulation, active power filters, hybrid active power filters, etc. He has coauthored two book and more than 100 journal and conference papers.

Dr. Wong received the Young Scientist Award from the "Instituto Internacional De Macau" in 2000, the Young Scholar Award from the University of Macau in 2001, second prize of the Tsinghua University Excellent Doctor Thesis Award in 2003, and third prize awards of the Invention Award of the Macau Government Science and Development Award in 2012 and 2014.